Optical Review (2022) 29:188–196
https://doi.org/10.1007/s10043-022-00733-4

REGULAR PAPER

Precise retinal shape measurement by alignment error and eye model calibration

Kseniya Palchunova[1] · Toshihiro Mino[2] · Toshifumi Mihashi[3] · Jonathan Liu[4] · Kuniharu Tasaki[5] · Yumi Hasegawa[5] · Takahiro Hiraoka[5] · Tetsuro Oshika[5]

Received: 28 December 2021 / Accepted: 29 March 2022 / Published online: 29 April 2022

Abstract

Objective To evaluate the repeatability of the optical coherence tomography (OCT) retinal shape measurement with and without alignment correction in children and adults.

Methods 62 eyes of the 31 subjects were examined on the OCT with auto-alignment and alignment correction functions. We performed three measurements on each eye, created 2D retinal height maps, and extracted horizontal and vertical profiles for repeatability analysis and Legendre polynomial representation. Repeatability was determined from the average standard deviation. We estimated the refractive errors produced by the observed alignment errors. We also examined the repeatability improvement of the slopes, curvatures, and higher-order coefficients for the subjects using the Student *t* test.

Results Repeatability was higher in the data with alignment. We observed the average repeatability in the child group with standard deviation (SD) equal 38.20 μm in raw data, and SD = 6.11 μm in the corrected data, in adults SD = 17.04 μm in raw data, and SD = 5.22 μm in the corrected data. The slope repeatability improved in both child [horizontal $t\,(18) = 4.62$, $p < 0.001$ and vertical $t\,(17) = 4.43$, $p < 0.001$] and adult groups [$t\,(18) = 2.73$, $p = 0.007$ and vertical $t\,(26) = 2.14$, $p = 0.02$], while higher-order coefficients were not affected.

Conclusions Alignment correction improved repeatability of the OCT retinal shape measurements, especially for child subjects. Curvature and higher-order distortions were not affected by the alignment error. The refractive errors produced by alignment errors are low, and the model can be used to estimate the peripheral refraction.

Keywords Optical coherence tomography · Retinal shape · Myopia · Repeatability · Peripheral refraction

✉ Toshifumi Mihashi
tmihashi@live.jp

Kseniya Palchunova
sharkuasriel@gmail.com

Toshihiro Mino
tmino@topcon.com

Jonathan Liu
jliu@topcon.com

Kuniharu Tasaki
k.tasaki1986@gmail.com

Yumi Hasegawa
tam_y110@yahoo.co.jp

Takahiro Hiraoka
thiraoka@md.tsukuba.ac.jp

Tetsuro Oshika
oshika@eye.ac

[1] Doctoral Program in Clinical Sciences, University of Tsukuba, Tsukuba, Japan

[2] R&D Department, Topcon Co, Tokyo, Japan

[3] Department of Orthoptics, Faculty of Medical Technology, Teikyo University, 2-11-1 Kaga, Itabashi, Tokyo 173-8605, Japan

[4] R&D Department, Topcon Co, Oakland, NJ, USA

[5] Department of Ophthalmology, University of Tsukuba, Tsukuba, Japan

1 Introduction

Myopia, as one of the most prevalent eye diseases worldwide [1], is drawing the increasing interest of clinicians and researchers. The prevalence of myopia is such that it has reached 80–90% among young adults in East and Southeast Asia [2, 3], and it has been estimated that it will affect nearly 50% of the world population by the year 2050 [4]. Regular monitoring of the myopic changes in the eye is crucial for effective treatment and slowing the progression of the condition. Moreover, effective monitoring solutions can help prevent various complications, such as myopic macular degeneration, retinal detachment, cataract, and glaucoma [5], and hence lower the risk of blindness as an outcome.

Currently, the gold standard of myopia screening includes refraction and axial length as parameters [6, 7], however, several studies have found significant shape distortions in myopic eyes [8–10], making longitudinal observation of the changes in the retinal shape a promising tactic. For the screening, we need a quick, accurate, and cost-effective method of imaging and analyzing eye shape and retinal shape in particular. In recent years magnetic resonance imaging (MRI) has been broadly used to model the eye shape [11–13] and explore any possible relationship with myopia [14–16]. However, the low accessibility of this method in clinical practice required finding an alternative. Therefore, optical coherence tomography (OCT) imaging has become a prospective solution for its daily use in clinical practice and higher image resolution. Subsequent studies have confirmed that OCT modeling can replace the use of MRI for posterior eye shape [17]. OCT imaging potentially allows for the creation of a model of the whole eye [18], as well as for the estimation of the peripheral refraction.

The effect of the peripheral retina on refraction development has been studied for more than five decades [19], to find a method to prevent ocular shape changes and therefore forming of the refractive error. Using simple lenses without consideration of peripheral refraction for myopia management imposes hyperopic defocus on the peripheral retina, which can lead to myopic growth and progression of myopia [20, 21]. However, peripheral defocus-modifying contact lenses are able to slow and even reverse the myopic eye growth [22, 23], by creating myopic defocus. Orthokeratology also modifies peripheral refraction as a therapeutic effect [24]. Knowledge of the precise retinal shape can aid the precision of the lens prescription and evaluation of the effectiveness of the treatment.

The retina may have some tilt against the anterior part of the eye. Unfortunately, conventional OCT measurements of the eye shape cannot evaluate the tilt of the retina because the retinal tilt in the OCT varies depending on the alignment of the OCT device to the eye. In the present study, we are introducing correction of the tilt distortion due to alignment error for precise analysis of OCT retinal shape. We are showing the improvement of the repeatability of the measurement with alignment correction, which potentially allows us to study the retina shape free of distortions. We are also presenting the accuracy of the tilt correction evaluated through a higher-order polynomial fitting.

2 Subjects and methods

2.1 Participants

We performed a prospective study of the subjects with different levels of refractive errors recruited from the Department of Ophthalmology at the University of Tsukuba Hospital, Japan. The study was approved by the Institutional Review Board of the University of Tsukuba. The present research followed the tenets of the Declaration of Helsinki. The operator (clinician or researcher) explained the nature of the experiment and the terms of personal data use and obtained informed consent from adult patients and parents or legal representatives of child patients before the measurements were obtained.

The data of 62 eyes of 31 healthy subjects were used for the analysis. The study included 17 children between the ages of 8–13 (mean age 11.00 ± 1.22 years) and 14 adults between the ages of 23–62 (mean age 39.01 ± 13.22 years). The refractive errors varied in the child group from -6.11D to -0.70D [mean spherical equivalent (SE) -3.31 ± 1.81D] and from -7.32 to 0.52 in the adult group (mean SE -3.20 ± 2.44D). The inclusion criteria for the subjects were that they were between 7 and 65 years old. A history of surgical myopia correction, as well as the presence of any inflammatory eye diseases, were exclusion criteria.

2.2 Measurements and instruments

All of the measurements were performed on non-dilated pupils. Eye fundus was scanned by a commercial spectral-domain OCT (3D-OCT-1, Topcon, Japan) with an auto-alignment function. The commercial device provides OCT volume data and alignment information, during measurement. The custom prototype software (Topcon, Japan) developed for this study was used to correct OCT shape in post-process due to alignment error during measurement, which is explained in detail in the following section. We define the correction as alignment correction in this study. The assessment included the objective refraction and keratometry data from a Hartmann-shack wavefront aberrometer

(KR-1 W, Topcon, Japan), an axial length from a low coherence interferometer biometry (IOLMaster 700, Carl Zeiss Meditec AG, Germany), and an open-view refractometer (WAM-5500, Shigiya, Japan).

2.3 Alignment correction

The main error source of the OCT retinal shape measurements is the alignment error of the difference between the entrance pupil center and the scanning pivot point of OCT probing light. OCT measures not physical shape but optical path length, and, therefore, OCT image is distorted by alignment errors and anterior eye optics. Optical distortion correction was devised using a commercial ray-tracing analysis program (CodeV, Synopsys, inc. USA) and the Gullstrand eye model [25]. Figure 1(A) and (B) represent the cases where an alignment error of 500 μm exists along the lateral and axial direction. We can see that OCT image deformation is more sensitive to lateral alignment error which is corrected by the alignment correction function developed for this study.

As commercially available feature, the OCT used in this research has stereo cameras to get and record the alignment error in 3-dimensions (Fig. 2). The stereo cameras are built-in at both the sides of the objective lens tilted against the OCT optical axis and take images of the anterior eye from left-side and right-side views. The entrance pupil position of the eye is analyzed from the anterior images, and the position is analyzed based on the disparity of two images taken by both cameras. The theoretical resolution of the alignment measurement is 44 μm in a lateral direction and 25 μm in an axial direction. The built-in commercial function of auto-alignment adjusts the instrument position so that the alignment error is minimized. The auto-alignment function is deactivated during OCT data acquisition, and residual alignment error exists during measurement, which reduces the reproducibility of shape measurement in OCT. The alignment error during OCT measurements is saved at 30 Hz. Then, cubic interpolation is used to calculate the alignment error for each B-frame. In post-process, the alignment correction function calculates OCT distortion corresponding to the recorded alignment error and corrects the distortion for every B-frame.

2.4 OCT imaging protocol

The images were collected using the fully automatic OCT with auto-alignment function. The size and definition of the raw images are horizontal 12 mm by vertical 9 mm. We performed OCT imaging with a horizontal scan mode and vertical scan mode to obtain reliable data considering possible eye movements. For the horizontal scan mode, the number of horizontal scans is 128 and each included 512 A-scans. For a vertical scan mode, the number of vertical scans is 128 and each included 512 A-scans. Alignment correction software then was used to create distortion-corrected data and resize it to 512 × 384 pixels over 12 × 9 mm. A merged 2D map was generated by combining the resized data acquired with horizontal-scan and vertical scan. The subjects from both the children and adult groups underwent the pair of horizontal- and vertical-scan-mode measurements 3 times for each eye. The subjects were instructed to keep their heads steady during imaging sessions, refrain from blinking while scans were taken, and rest their eye between each acquisition. The scans containing artifacts or blinking within 3 mm radius centered at the fovea in the en face 2D map were discarded

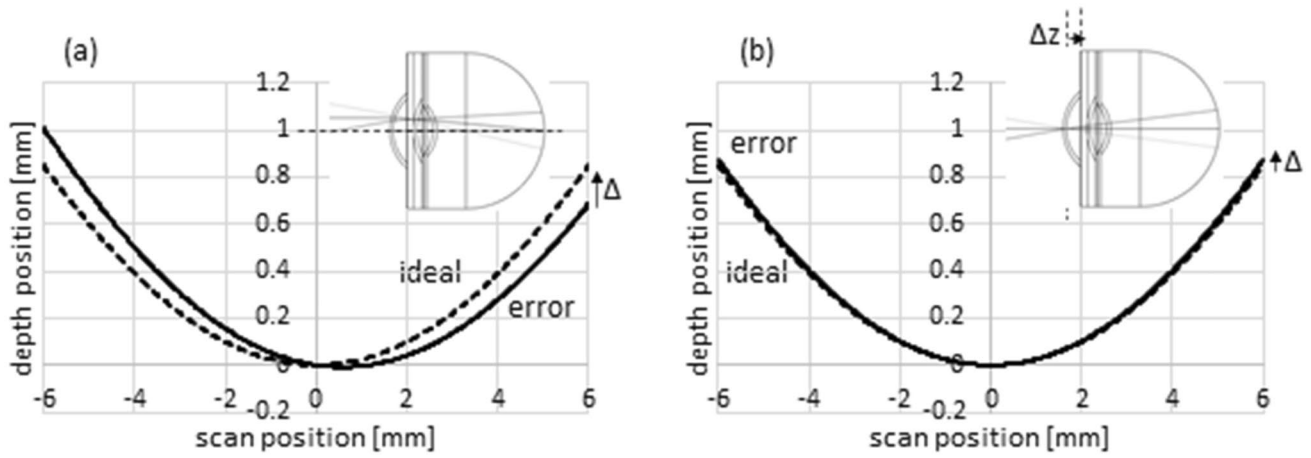

Fig. 1 Modeling of OCT profile deformation by alignment error. (A, B) Schematic illustration of alignment error and OCT profile change. Solid lines indicate OCT retinal shape profiles taken under ideal configuration with no alignment error of relative position between system and eye. Dashed lines indicate OCT retinal shape profiles taken with an alignment error of Δ = 500 μm **a** along the lateral direction and **b** along the axial direction

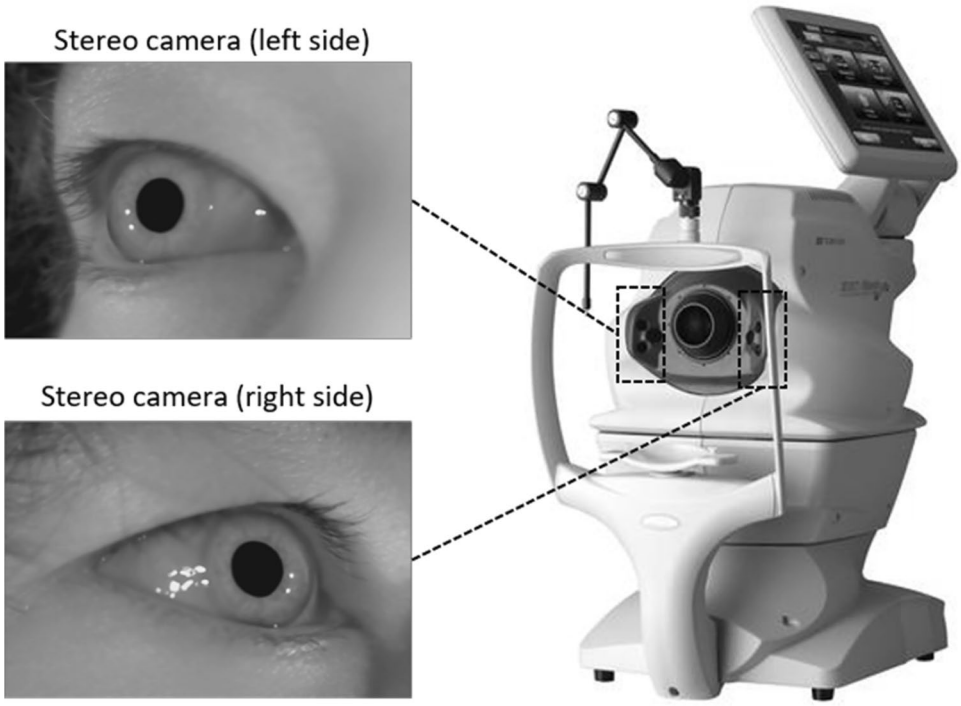

Fig. 2 Image of the OCT device used in the study and the photographic demonstration of the position of the stereo cameras and their view angle

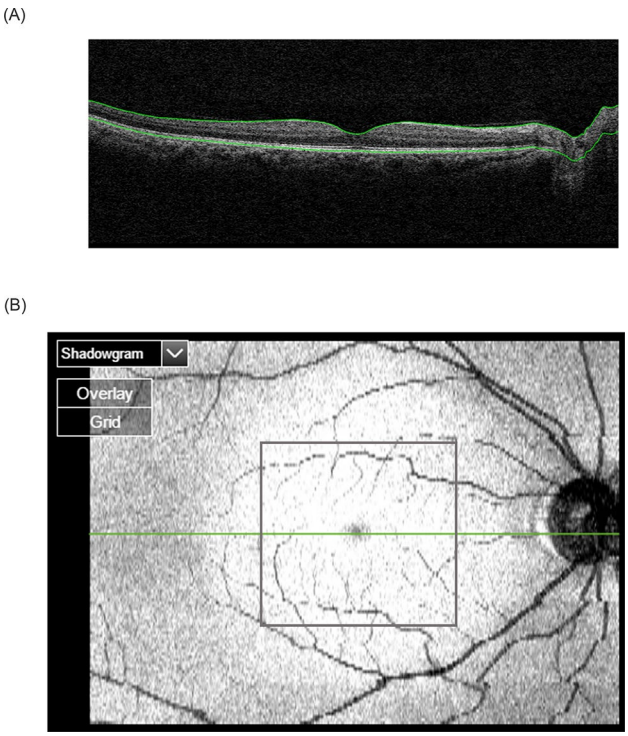

Fig. 3 Sample images of one measurement taken with OCT device. **A** OCT fundus image with RPE segmentation line (lower green line). **B** Fundus image. The square shows an area used in the analysis (±3 mm from the fovea center)

and retaken (Fig. 3). The OCT procedure was performed on a non-dilated pupil with no glasses and contact lenses.

2.5 Retinal shape representation

The retinal pigment epithelium (RPE) segmented line was obtained from OCT B-scan images with commercial software (IMAGEnet6, Topcon, Japan) and was defined as retinal shape. Fovea center was chosen as a central point in this model, where $x = 0, y = 0$ at the fovea center, with x indicating the horizontal and y the vertical position. The retinal OCT height $H_{\mathrm{OCT}}(x, y)$ was calculated based on the RPE segmentation line at the fovea center as

$$H_{\mathrm{OCT}}(x, y) = \mathrm{OPL}_{\mathrm{RPE}}(0, 0) - \mathrm{OPL}_{\mathrm{RPE}}(x, y)$$

$\mathrm{OPL}_{\mathrm{RPE}}(x, y)$ is optical path length to RPE at the position x, y. The RPE height data corresponding to the vertical and horizontal central sections was chosen for the analysis and defined as vertical and horizontal profiles respectively.

We also represented the retinal shape using curve estimation, to study the repeatability of the slope, curvature, and the 3rd and 4th order coefficients between the scans in raw and aligned data using the Legendre polynomial fitting [26]. We omitted the parts of the profiles corresponding to the optic nerve head and the image edges. We adjusted all profiles to be close to the same size in tissue (8.68 ± 0.01 mm) for the most accurate comparison.

2.6 Statistical analysis

We used the data of the right eyes for representation. For the evaluation of the measurement precision, we checked the standard deviation (SD) among the horizontal and vertical profiles from the data of 3 measurements. We used the data points 3 mm from the fovea for analysis, therefore omitting the optic nerve head (ONH) area, since the RPE segmentation is not reliable around the ONH area. The profiles were extracted from the 2D maps, which represent the numerical values of the OCT retinal height, and were created using the prototype software (Topcon Co, Japan). We compared the repeatability in the profiles of the raw data with the data after the software alignment correction. We also compared child and adult data to investigate the efficacy and limitations of the measurement in children. We estimated the repeatability of refraction measurements from the repeatability of the OCT retinal height measurements using the formula,

(SD of refraction) = (SD of OCT retinal height) × (average refractive power = 60 D)/(average axial length = 24 mm).

Moreover, we compared the standard deviations of the polynomial coefficients obtained from the data of 3 measurements, with and without alignment correction in each group and section using a paired two-sample *t* test. We also demonstrated the change of the coefficient repeatability as the difference of the SD, which was defined as the SD of Legendre polynomial coefficients before the numerical motion correction subtracted by that after the correction.

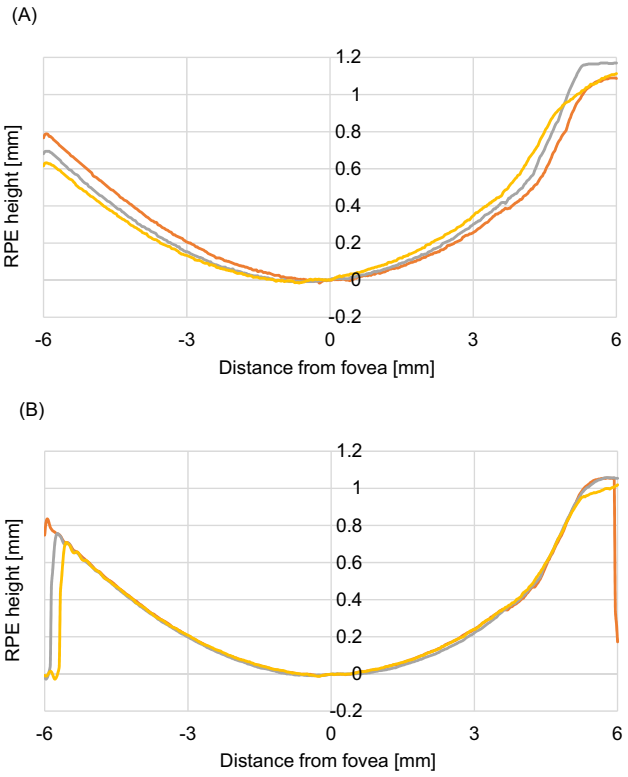

Fig. 4 Whole horizontal profiles of three repeated measurements from a sample child data. **A** The data without alignment correction. **B** The data with alignment correction. Abbreviation: *RPE* retinal pigment epithelium

3 Results

The tilt correction helped to significantly improve the precision of the measurement. Figure 4 shows whole horizontal profiles obtained from one of our child measurement data with and without alignment correction.

Table 1 shows height repeatability at 3 mm point from the macular center for each group and scan direction, and an expected refractive error produced by the alignment errors.

We observed the best repeatability in the horizontal scans in the child group (5.86 μm) and the vertical scan in the adult group (4.61 μm). The maximal average SD in the compensated retinal shape measurements was 6.36 μm in the child group and 5.82 μm in the adult group, which were corresponding to 0.016D and 0.015D in spherical errors in refraction, respectively.

Alignment errors occurred in a few cases, especially in the vertical profiles in child groups, where head movements created large differences in the z-position of the scans, producing significant differences between the measurements; however, software correction normalized the retina position on the scans, therefore decreasing the error and creating high average repeatability in all sections. Therefore, the difference between the repeatability in the vertical and horizontal scans in the raw data is likely caused by the effect of the alignment error (Fig. 5).

Repeatability of the slopes has improved significantly after alignment correction in the adult group in both horizontal [$t\,(18) = 4.62$, $p < 0.001$] and vertical [$t\,(17) = 4.43$, $p < 0.001$], as well as in the child group in both horizontal [$t\,(18) = 2.73$, $p = 0.007$] and vertical [$t\,(26) = 2.14$, $p = 0.02$] profiles (Table 2). Curvatures and higher-order coefficients did not change significantly. Figure 6 shows the difference of SD of the coefficients in 3 measurements between the data with and without alignment correction for each subject.

4 Discussion

Good repeatability of height measurements of retinal shapes after alignment calibration was observed for both child and adult eyes. The repeatability is good enough to predict off-axis refraction by simulation with retinal shape.

In raw OCT height data, the repeatability of child measurements was 2.24 times worse than that of adults. In 5 cases significant alignment errors were observed in child

Table 1 Repeatability of the OCT retinal height measurement values and estimated refractive errors

	OCT height data with correction, µm	Refractive error, D	Raw OCT height data, µm	Refractive error, D
Adults				
Horizontal	5.82	0.015	19.84	0.050
Vertical	4.61	0.012	14.25	0.036
Children				
Horizontal	5.86	0.015	24.34	0.061
Vertical	6.36	0.016	52.06	1.030

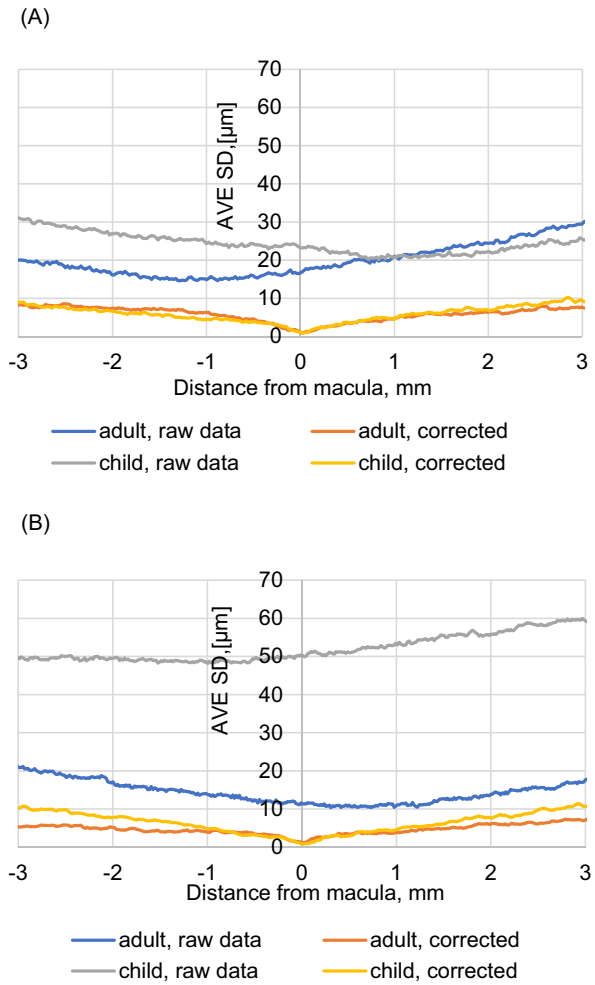

Fig. 5 Average repeatability of the OCT retinal height measurements in child and adult groups with and without alignment correction. **A** Average standard deviation (AVE SD) in the horizontal profiles. **B** Average SD in the vertical profiles. Abbreviation: *AVE SD* average standard deviation

data before correction. In these cases, large alignment errors occurred in the optical axis direction. One of the possible reasons is the physiologically lower ability to maintain fixation on a target [27] during the measurements. Other errors we found in image processing, which occurred not only in child measurements but also in adult measurements, were caused by artifacts and eye movements, undetected on the primary image quality screening performed by the operator.

In the present stage of the study, we discovered certain limitations in using the technique in children. Apart from the above-mentioned physiological properties, the behavioral difference in children can affect the result's quality, such as a short period of concentration on the procedure and decreasing control over eye and body movements during the repeated measurements. Children also might need assistance in keeping the correct head position between and during the measurements, due to their higher reactivity to distractions appearing in the clinic environment and the fatigue caused by the unusual circumstances. Nevertheless, the obtained results show good efficacy of the alignment correction and seem promising for further investigation.

The repeatability of slopes improved in both groups after the correction, however, we observed no significant change in the curvature and higher-order coefficients. In the analysis, we omitted the ONH area, due to the disruption of RPE, as well as the edges of the images since the compensation of eye movements and adjustment of the macular center caused a small image shift. However, it didn't affect the reliability of the polynomial fitting. We were able to include the area further than 3 mm from the macula because the Legendre fitting allowed us to ignore small height aberrations.

Lateral alignment error induces asymmetric distortion and axial alignment error affects curvature in OCT images. While creating the model, we found that OCT profiles are more sensitive to lateral alignment errors than axial alignment errors. The theoretical considerations perfectly explain our measurement results in which we found large repeatability errors in raw data, caused mainly by the tilt errors. Furthermore, those errors were corrected by the calibration method using alignment error measurement data during OCT scanning.

Table 2 Comparison of repeatability of the Legendre polynomial coefficients

Coefficient order			1st	2nd	3rd	4th
Child data	Horizontal	SD aligned	9.391	2.402	1.339	1.309
		SD raw	24.391	2.905	1.748	1.592
		t test	2.74, $p=0.01$	0.79, $p=0.22$	1.20, $p=0.12$	0.76, $p=0.23$
	Vertical	SD aligned	9.925	4.012	1.705	2.047
		SD raw	22.363	4.463	2.644	1.831
		t test	2.14, $p=0.02$	0.41, $p=0.34$	1.81, $p=0.04$	0.46, $p=0.33$
Adult data	Horizontal	SD aligned	4.992	2.073	2.190	1.314
		SD raw	19.219	2.570	2.139	1.426
		t test	4.62, $p<0.001$	1.02, $p=0.16$	0.09, $p=0.46$	0.45, $p=0.33$
	Vertical	SD aligned	5.586	1.783	1.260	1.226
		SD raw	17.697	1.815	1.080	1.131
		t test	4.43, $p<0.001$	0.09, $p=0.47$	0.46, $p=1.71$	0.34, $p=0.37$

SD standard deviation

As we introduced, myopia has been intensively studied concerning both its progression and prevention. Some of the prevention methods, including orthokeratology and low dose atropine, have been proven to be effective in slowing myopia progression. Standard myopia screening methods are objective refraction and axial length measurements. The retinal shape is one of the candidates for early detection and prediction of myopia progression. Verkicharla et al. proposed the classification of retinal shapes [28], which they observed after collecting the clinical data on off-axis refraction. They found asymmetry in the retinal shape, and good repeatability of the slope measurement of the retinal profile would be crucial for detecting this. OCT retinal shape measurement is readily available for clinical screening using our correction method, and it can measure both horizontal profiles and vertical profiles.

The reported results were obtained in the preliminary stage of the study; we estimated repeatability from analysis in which we did not fully use our clinical data. For example, we did not use axial length for the calibration. To obtain the model of a true retinal shape, we need to consider the axial length, refraction, and keratometry.

Our next goal will be estimating peripheral refraction from the OCT retinal shape. For this purpose, we will need accurate retinal shape measurements. We will achieve this by considering the axial length and keratometry data we obtained during measurements. Meanwhile, we confirmed the repeatability of retinal height measurement is 5.7 μm with SD evaluation and this will be corresponding to the precision of refractive error estimation, which is 0.014 D.

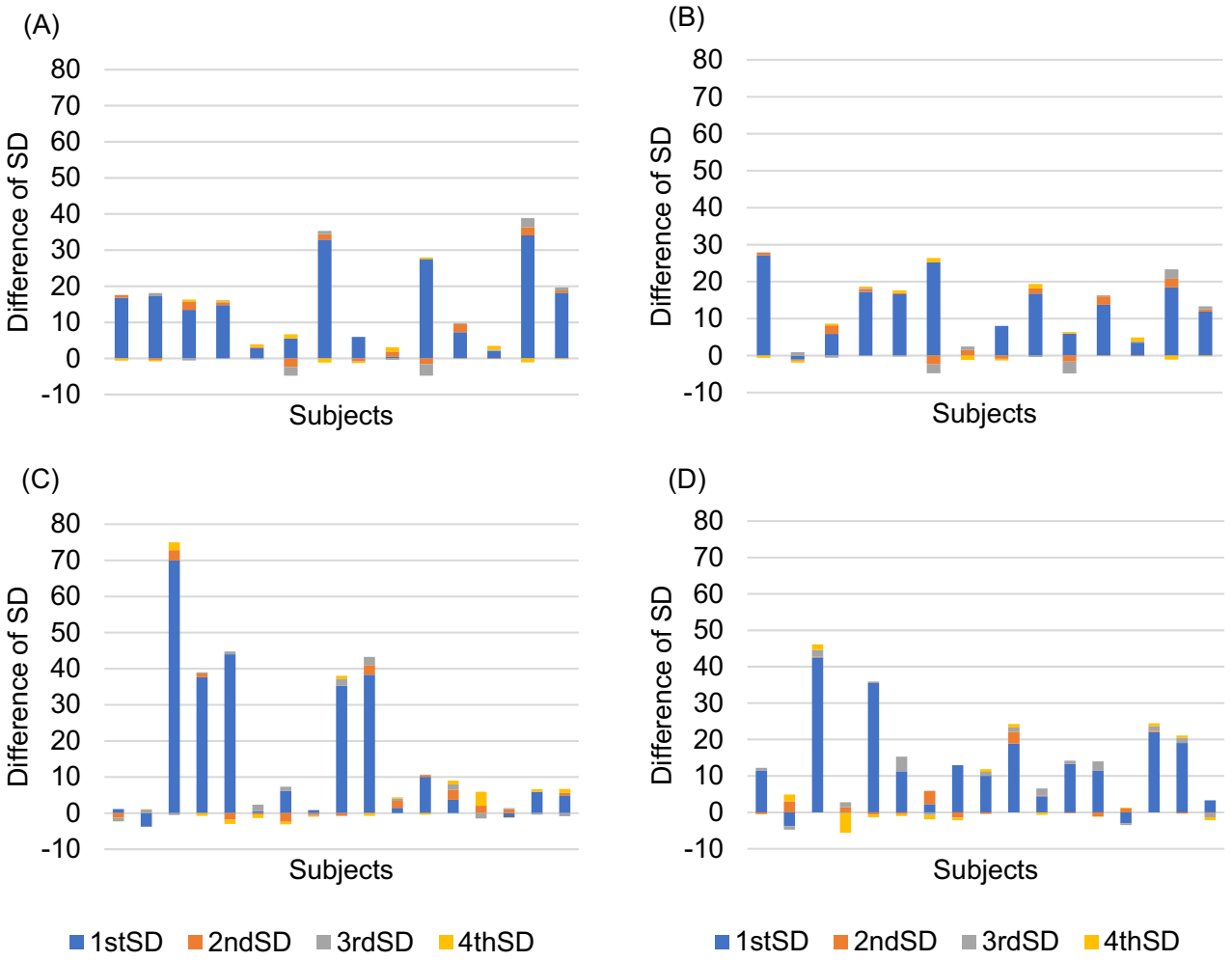

Fig. 6 Coefficient repeatability change between raw and aligned data. **A** Horizontal profiles of the adult group. **B** Vertical profiles of the adult group. **C** Horizontal profiles of the child group. **D** Vertical profiles of the child group. The positive y scale corresponds to the improvement of the repeatability with alignment, while the negative difference indicates the repeatability in aligned data got worse. Abbreviation: *SD* standard deviation

Acknowledgements This work was supported by the R&D Department, Topcon Co, Tokyo, Japan, and the Department of Ophthalmology at the University of Tsukuba, Tsukuba, Japan. The sponsor did not influence the research outcomes.

Author contributions Commercial relationships: Topcon Co: TM (E), JL (E), TO (F).

References

1. Foster, P.J., Jiang, Y.: Epidemiology of myopia. Eye (Basingstoke). **28**, 202–208 (2014). https://doi.org/10.1038/eye.2013.280
2. Wu, P.-C., Huang, H.-M., Yu, H.-J., Fang, P.-C., Chen, C.-T.: Epidemiology of Myopia. Asia-Pac. J. Ophthalmol. **5**, 386–393 (2016). https://doi.org/10.1097/APO.0000000000000236
3. Morgan, I.G., French, A.N., Ashby, R.S., Guo, X., Ding, X., He, M., Rose, K.A.: The epidemics of myopia: aetiology and prevention. Prog. Retinal. Eye. Res. **62**, 134–149 (2018). https://doi.org/10.1097/10.1016/j.preteyeres.2017.09.004
4. Holden, B.A., Fricke, T.R., Wilson, D.A., Jong, M., Naidoo, K.S., Sankaridurg, P., Wong, T.Y., Naduvilath, T.J., Resnikoff, S.: Global prevalence of myopia and high myopia and temporal trends from 2000 through 2050. Ophthalmology. **123**, 1036–1042 (2016). https://doi.org/10.1016/j.ophtha.2016.01.006
5. Haarman, A.E.G., Enthoven, C.A., Willem Tideman, J.L., Tedja, M.S., Verhoeven, V.J.M., Klaver, C.C.W.: The complications of myopia: a review and meta-analysis. Investig. Ophthalmol. Vis. Sci. **61**(4), 49 (2020). https://doi.org/10.1016/10.1167/iovs.61.4.49
6. American Optometric Association. Evidence-based clinical practice guideline: comprehensive pediatric eye and vision

examination. Optom. Clin. Pract. **2**(2) (2020). https://doi.org/10.37685/uiwlibraries.2575-7717.2.2.1007
7. Wolffsohn, J.S., Flitcroft, D.I., Gifford, K.L., Jong, M., Jones, L., Klaver, C.C.W., Logan, N.S., Naidoo, K., Resnikoff, S., Sankaridurg, P., Smith, E.L., Troilo, D., Wildsoet, C.F.: IMI—myopia control reports overview and introduction. Invest. Ophthalmol. Vis. Sci. **60**, M1–M19 (2019). https://doi.org/10.1167/iovs.18-25980
8. Atchison, D.A., Jones, C.E., Schmid, K.L., Pritchard, N., Pope, J.M., Strugnell, W.E., Riley, R.A.: Eye shape in emmetropia and myopia. Invest. Ophthalmol. Vis. Sci. **45**, 3380–3386 (2004). https://doi.org/10.1167/iovs.04-0292
9. Guo, X., Xiao, O., Chen, Y., Wu, H., Chen, L., Morgan, I.G., He, M.: Three-dimensional eye shape, myopic maculopathy, and visual acuity: the zhongshan ophthalmic center-brien holden vision institute high myopia cohort study. Ophthalmology **124**, 679–687 (2017). https://doi.org/10.1016/j.ophtha.2017.01.009
10. Wakazono, T., Yamashiro, K., Miyake, M., Hata, M., Miyata, M., Uji, A., Nakanishi, H., Oishi, A., Tamura, H., Ooto, S., Tsujikawa, A.: Time-course change in eye shape and development of staphyloma in highly myopic eyes. Invest. Ophthalmol. Vis. Sci. **59**, 5455–5461 (2018). https://doi.org/10.1167/iovs.18-24754
11. Ciller, C., Zanet, D., Rüegsegger, S.I., Pica, M.B., Sznitman, A., Thiran, R., Maeder, J.-P., Munier, P.L., Kowal, F.L., Cuadra, J.H.: Automatic segmentation of the eye in 3D magnetic resonance imaging: a novel statistical shape model for treatment planning of retinoblastoma. Int. J. Radiat. Oncol. Biol. Phys. (2015). https://doi.org/10.7892/boris.65805
12. Lim, L.S., Yang, X., Gazzard, G., Lin, X., Sng, C., Saw, S.M., Qiu, A.: Variations in eye volume, surface area, and shape with refractive error in young children by magnetic resonance imaging analysis. Invest. Ophthalmol. Vis. Sci. **52**, 8878–8883 (2011). https://doi.org/10.1167/iovs.11-7269
13. Lee, K.M., Park, S.W., Kim, M., Oh, S., Kim, S.H.: Relationship between three-dimensional magnetic resonance imaging eyeball shape and optic nerve head morphology. Ophthalmology. **128**, 532–544 (2021). https://doi.org/10.1016/j.ophtha.2020.08.034
14. Moriyama, M., Ohno-Matsui, K., Hayashi, K., Shimada, N., Yoshida, T., Tokoro, T., Morita, I.: Topographic analyses of shape of eyes with pathologic myopia by high-resolution three-dimensional magnetic resonance imaging. Ophthalmology. **118**, 1626–1637 (2011). https://doi.org/10.1016/j.ophtha.2011.01.018
15. Pope, J.M., Verkicharla, P.K., Sepehrband, F., Suheimat, M., Schmid, K.L., Atchison, D.A.: Three-dimensional MRI study of the relationship between eye dimensions, retinal shape and myopia. Biomed. Opt. Express. **8**, 2386 (2017). https://doi.org/10.1364/boe.8.002386
16. Ohno-Matsui, K., Akiba, M., Modegi, T., Tomita, M., Ishibashi, T., Tokoro, T., Moriyama, M.: Association between shape of sclera and myopic retinochoroidal lesions in patients with pathologic myopia. Invest. Ophthalmol. Vis. Sci. **53**, 6046–6061 (2012). https://doi.org/10.1167/iovs.12-10161
17. Kuo, A.N., Verkicharla, P.K., McNabb, R.P., Cheung, C.Y., Hilal, S., Farsiu, S., Chen, C., Wong, T.Y., Kamran Ikram, M., Cheng, C.Y., Young, T.L., Saw, S.M., Izatt, J.A.: Posterior eye shape measurement with retinal OCT compared to MRI. Invest. Ophthalmol. Vis. Sci. (2016). https://doi.org/10.1167/iovs.15-18886
18. Kuo, A.N., McNabb, R.P., Izatt, J.A.: Advances in whole-eye optical coherence tomography imaging. Asia. Pac. J. Ophthalmol. **8**(2), 99–104 (2019). https://doi.org/10.22608/APO.201901
19. Atchison, D.A., Pritchard, N., Schmid, K.L.: Peripheral refraction along the horizontal and vertical visual fields in myopia. Vision. Res. **46**, 1450–1458 (2006). https://doi.org/10.1016/j.visres.2005.10.023
20. Benavente-Pérez, A., Nour, A., Troilo, D.: Axial eye growth and refractive error development can be modified by exposing the peripheral retina to relative myopic or hyperopic defocus. Invest. Ophthalmol. Vis. Sci. **55**, 6765–6773 (2014). https://doi.org/10.1167/iovs.14-14524
21. Smith, E.L., Hung, L.F., Huang, J., Blasdel, T.L., Humbird, T.L., Bockhorst, K.H.: Effects of optical defocus on refractive development in monkeys: evidence for local, regionally selective mechanisms. Invest. Ophthalmol. Vis. Sci. **51**, 3864–3873 (2010). https://doi.org/10.1167/iovs.09-4969
22. Zhang, H.Y., Lam, C.S.Y., Tang, W.C., Leung, M., To, C.H.: Defocus incorporated multiple segments spectacle lenses changed the relative peripheral refraction: A 2-year randomized clinical trial. Invest. Ophthalmol. Vis. Sci. (2020). https://doi.org/10.1167/IOVS.61.5.53
23. Zhu, Q., Liu, Y., Tighe, S., Zhu, Y., Su, X., Lu, F., Hu, M.: Retardation of myopia progression by multifocal soft contact lenses. Int. J. Med. Sci. **16**(2), 198–202 (2019). https://doi.org/10.7150/ijms.30118
24. Gifford, K.L., Gifford, P., Hendicott, P.L., Schmid, K.L.: Stability of peripheral refraction changes in orthokeratology for myopia. Cont. Lens Anterior. Eye. **43**, 44–53 (2020). https://doi.org/10.1016/j.clae.2019.11.008
25. von Helmholtz, H.: Helmholtz`s treatise on physiological optics. Thoemmes Continuum, Bristol (2000)
26. Aboites, V.: Legendre polynomials: a simple methodology. J. Phys. Conf. Ser. (2019). https://doi.org/10.1088/1742-6596/1221/1/012035
27. Helo, A., Pannasch, S., Sirri, L., Rämä, P.: The maturation of eye movement behavior: scene viewing characteristics in children and adults. Vision. Res. **103**, 83–91 (2014). https://doi.org/10.1016/j.visres.2014.08.006
28. Verkicharla, P.K., Mathur, A., Mallen, E.A.H., Pope, J.M., Atchison, D.A.: Eye shape and retinal shape, and their relation to peripheral refraction. Ophthalmic. Physiol. Opt. **32**(3), 184–199 (2012). https://doi.org/10.1111/j.1475-1313.2012.00906.x